Remarks on crack-bridging concepts

G Bao

Mechanical Engineering Department, The Johns Hopkins University, Baltimore MD 21218

Z Suo

Department of Mechanical and Environmental Engineering, The University of California, Santa Barbara CA 93106

The article draws upon recent work by us and our colleagues on metal and ceramic matrix composites for high temperature engines. The central theme here is to deduce mechanical properties, such as toughness, strength and notch-ductility, from bridging laws that characterize inelastic processes associated with fracture. A particular set of normalization is introduced to present the design charts, segregating the roles played by the shape, and the scale, of a bridging law. A single material length, $\delta_0 E / \sigma_0$, emerges, where δ_0 is the limiting-separation, σ_0 the bridging-strength, and E the Young's modulus of the solid. It is the huge variation of this length—from a few nanometers for atomic bond, to a meter for cross-over fibers—that underlies the richness in material behaviors. Under small-scale bridging conditions, $\delta_0 E / \sigma_0$ is the only basic length scale in the mechanics problem and represents, with a pre-factor about 0.4, the bridging zone size. A catalog of small-scale bridging solutions is compiled for idealized bridging laws. Large-scale bridging introduces a dimensionless group, $a/(\delta_0 E / \sigma_0)$, where a is a length characterizing the component (e.g., hole radius). The group plays a major role in all phenomena associated with bridging, and provides a focus of discussion in this article. For example, it quantifies the bridging scale when a is the unbridged crack length, and notch-sensitivity when a is hole radius. The difference and the connection between Irwin's fracture mechanics and crack bridging concepts are discussed. It is demonstrated that fracture toughness and resistance curve are meaningful only when small-scale bridging conditions prevail, and therefore of limited use in design with composites. Many other mechanical properties of composites, such as strength and notch-sensitivity, can be simulated by invoking large-scale bridging concepts.

1. BACKGROUND

Building upon the analyses of Dugdale (1960) and Bilby *et al*. (1963), Cottrell (1963) put forward the concept of crack-bridging as a unifying theory for fracture at various length scales, from atomic cleavage to void growth. Much has happened in the last thirty years in developing this idea for all kinds of materials—metals, ceramics, polymers, cementitious materials, and their composites in various forms. In this article, we try to place the relevant aspects into the perspective of design *with*—and *of*—ceramic matrix composites. In particular, we will emphasize the concept of large-scale bridging, and its implications for strength, notch-sensitivity, and splitting resistance.

This section sets the stage for our remarks on crack bridging concepts. In particular, we briefly discuss bridging laws, the microscopic properties to be transmitted to continuum models. The fundamentals of Irwin's fracture mechanics are reviewed, motivating the models for toughness, and demonstrating the limitations of small-scale bridging. The section is concluded with comments on current practice of fracture testing, and needs for large-scale bridging concepts.

1.1 Atomic bond vs fiber bridging

A solid will fall apart unless something holds it together. For example, an ionic crystal adheres by electrostatic force between unlike ions. A unifying idea, sufficiently rigorous for our purpose, is to represent atomic bond by a relation between attractive stress, σ, and separation, δ, of two lattice planes. Such a relation is sketched in Fig. 1, and is formally written as

$$\sigma / \sigma_0 = \chi(\delta / \delta_0). \qquad (1)$$

The dimensionless function χ describes the *shape* of the relation; the *scale* is set by strength, σ_0, and limiting-separation, δ_0. For an inorganic solid, the strength is about

"Micromechanical modelling of quasi-brittle materials behavior" edited by Victor C Li, ASME Book No AMR118 $60 (members $30)
Appl Mech Rev vol 45, no 8, August 1992

one tenth of its Young's modulus, and the limiting-separation is on the order of lattice spacing (see Table 1).

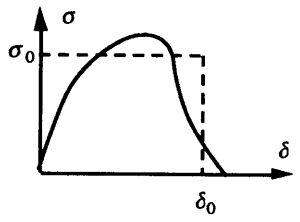

FIG. 1 A stress-separation relation that represents both atomic bond and fiber bridging. The strength and limiting-separation are very different for the two mechanisms; see Table 1.

TABLE 1 Illustrative properties for bridging mechanisms

	atomic bond	fiber pull-out	fiber cross-over
σ_0 (N/m^2)	10^{10}	10^9	10^7
δ_0 (m)	10^{-10}	10^{-5}	10^{-4}
$\sigma_0\delta_0$(J/m^2)	1	10^4	10^3
$\delta_0 E/\sigma_0$ (m)	10^{-9}	10^{-3}	1

As pointed out by Needleman (1990), relation (1) introduces a stress level σ_0 and a length scale δ_0, and provides an intrinsic failure criterion, based on which macroscopic phenomena can be simulated. Table 1 lists the values of $\sigma_0\delta_0$ and $\delta_0 E/\sigma_0$ (Young's modulus is taken to be $E \sim 10^{11}\mathrm{N/m^2}$). As we shall see later, they represent, with pre-factors of order unity, fracture energy and fracture process zone length, respectively, when the process zone is much smaller than flaw size. The significance of the length, $\delta_0 E/\sigma_0$, was first appreciated by Cottrell (1963), and will be further elaborated upon in this article in connection with composite design.

Things other than atomic bonds can also hold a material together. Illustrated in Fig. 2 are strong fibers bridging a ceramic matrix, mimicking atomic bonds holding a solid. By analyzing a fiber-matrix cylinder, one finds an approximate stress-separation relation (Marshall *et al.* 1985; also Hutchinson and Jensen 1990 for a correction):

$$\sigma/\sigma_0 = (\delta/\delta_0)^{1/2}. \tag{2}$$

The closure-strength is

$$\sigma_0 = fS_b, \tag{3}$$

where S_b is the fiber bundle strength, and f the fiber volume fraction. The limiting-separation is

$$\delta_0 = \frac{(1-f)^2 S_b^2}{2E\tau} R, \tag{4}$$

where R is the fiber radius, τ the sliding friction of fiber/matrix interface, and E the Young's modulus, assuming that elastic constants are identical for fiber and matrix. In practice, δ_0 can be varied substantially by varying τ.

Note that (2) is valid before fiber breaking. Fiber pull-out after breaking has also been modeled; see Hutchinson and Jensen (1990) for review. Yet design with ceramic matrix composites under static loading, and metal matrix composites under cyclic loading usually allows matrix cracking to relieve stress concentration, but requires fibers to remain intact, so that (2) provides a conservative limit in design.

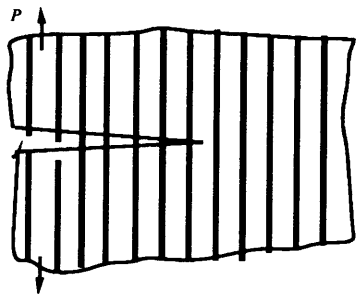

FIG. 2 Fiber pull-out.

Fibers can even bridge transverse cracks if they are not perfectly aligned (Fig. 3). High fracture resistance due to cross-over fibers has been demonstrated for a glass matrix composite (Spearing and Evans 1992). The stress-separation relation has not been modeled in any detail, but the flexible fibers are expected to provide small closure-strength and large limiting-separation. Values listed in Table 1 are inferred from the experimental data of a CAS/SiC composite.

Ductile, crack-bridging particles can substantially toughen a ceramic (e.g., Bannister *et al.* 1992). The closure-strength is a few times the yield stress of the ductile alloy, and the limit separation scales with the product of the size and the ultimate strain of the particles. They are also influenced by debonding of the particle/matrix interface (Mataga 1990, Bao and Hui 1990).

All bridging mechanisms can be represented by stress-separation relations, but there is a significant difference: the scales of σ_0 and δ_0. It is the large variation in the bridging scales, from a nanometer to a meter, that accounts for the richness in material behaviors. In particular, as indicated in Table 1, the fracture energy and damage extent differ substantially for atomic bond and fiber bridging.

Given a stress-separation relation that tells how a solid is held together, one can analyze any components to determine the load-carrying capacity, which is the approach to be reviewed in this article. However, this was *not* how Irwin established the Linear Elastic Fracture Mechanics. In fact, LEFM makes no reference to microscopic details of fracture process. To place bridging concepts into perspective, it is interesting, then, to first reflect upon the facts underlying the fracture *mechanics* that is independent of the fracture *mechanisms*. The classical view outlined below can be found in the textbook by Kanninen and Popelar (1985).

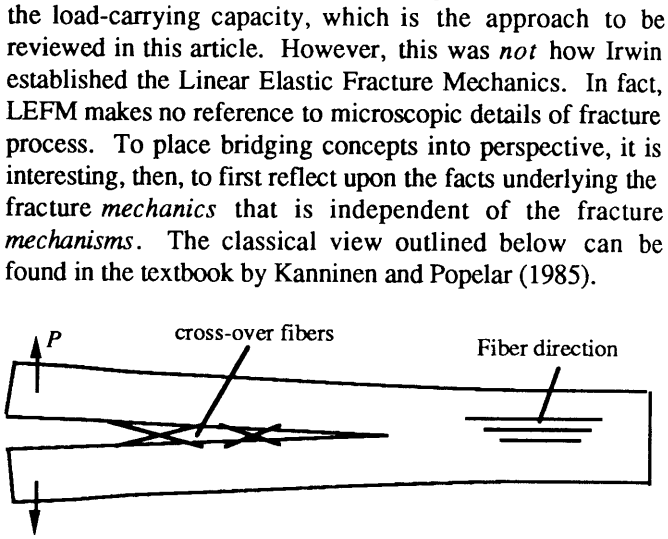

FIG. 3 Fiber cross-over.

1.2 Linear elastic fracture mechanics

Ironically, it is the very irrelevance to microscopic details that gave rise to the great success of fracture mechanics in the early days. LEFM is versatile: it applies, with some justifications, to any solids—metals, ceramics, polymers and composites. LEFM is precise: it relies on macroscopic measurements of toughness and elasticity solutions of stress intensity factors. LEFM is far-reaching: the concepts have been extended to ductile fracture, fatigue cracking, dynamic fracture, and interface debonding.

Irwin's LEFM erects upon a single premise: At the onset of fracture, the material is elastic over the whole component, except for a *damage zone* localized around the crack tip, whose size L_0 is much smaller than crack size a:

$$L_0 \ll a. \tag{5}$$

The condition is satisfied by either a large crack, or a brittle solid suffering little diffused damage upon fracture. This statement will be made more precise later

Then follows the central corollary: *However complex a fracture process is, a single material property (called toughness) quantifies the resistance to fracture.* That is, for a given material, toughness measured from a laboratory sample can be used to design components.

No microscopic details are mentioned.

The elastic field in a component is analyzed as if the crack tip—or the tiny inelastic zone—were a mathematical point with no physical structure, an idea analogous to the boundary layer approach in fluid mechanics. Such stress field is square root singular:

$$\sigma_{ij} \sim K(2\pi r)^{-1/2} F_{ij}(\theta), \tag{6}$$

where r and θ form polar coordinates centered at the crack tip, $F_{ij}(\theta)$ are functions listed in elasticity textbooks, and K is *stress intensity factor*. The external boundary conditions of the component do not change the structure of the singular field—the square root and functions $F_{ij}(\theta)$, but do change the magnitude of K.

The physical significance of K can be appreciated from Fig. 4. The actual stress distribution is modified in two ways from the elastic solution (6). Within the damage zone, the inelastic deformation redistributes stress, bounding the stress by the closure-strength, σ_0. Close to the component boundary, the stress merges to the boundary conditions. Despite the modifications, provided condition (5) is satisfied, the stress field within the annulus, $L_0 < r < a$, is well approximated by elastic solution (6).

Consequently, K is the *only parameter* through which the applied load can influence the damaging process at the crack tip. The resistance to fracture can therefore be defined as the maximum stress intensity factor that a material can sustain. That is, for a given cracked specimen made of a certain material, denoting K as the stress intensity factor of the *geometry and loading*, and K_c the toughness of the *material*, the crack will not grow if

$$K < K_c. \tag{7}$$

In contrast to other measures of toughness such as impact energy, K_c is both macroscopically measurable and quantitatively relevant to design. Two handbooks are thus sufficient: one contains stress intensity factors of various *geometries*, computed from elasticity problems; and the other contains toughness values for various *materials*, measured from laboratory samples.

No microscopic details are mentioned.

Another useful concept is energy release rate $\mathcal{G}$, the decrease of elastic strain energy of the body, for a unit area of crack growth, when the deflection at the external loading point is held fixed. Irwin (1957) showed that $\mathcal{G}$ and K are related by

$$\mathcal{G} = K^2 / E', \tag{8}$$

where $E' = E$ for plane stress, and $E' = E/(1 - \nu^2)$ for plane strain, E and ν being the Young's modulus and Poisson's ratio. Fracture energy Γ is related to K_c by a similar relation

$$\Gamma = K_c^2 / E'. \tag{9}$$

In summary, K and $\mathcal{G}$ are equivalent *loading parameters*; K_c and Γ are equivalent *material properties*. All these are valid concepts when small-scale damage condition (5) prevails.

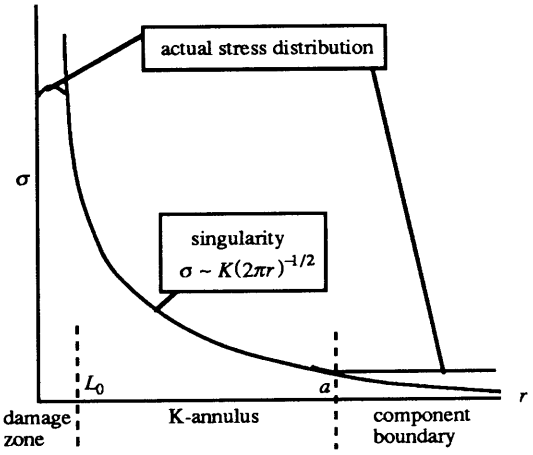

FIG. 4 Elastic solution and actual stress distribution.

1.3 Mechanics of toughness

Powerful as it is, LEFM uncovers little of what happens *within* the damage zone. There is a number of disadvantages of this black-box approach. For one, toughness can be enhanced by controlling microstructure; it is of great significance to have a theory for toughness, so that the controllable quantities can be optimized. This theme has been vigorously pursued for the past twenty years, culminating in an understanding of toughness—to various degrees of sophistication—for almost all engineering materials. For example, the microstructural basis of toughness has been reviewed by Evans (1990) for ceramics, by Ritchie and Thompson (1985) for ductile alloys, and by Li (1990) for cementitious materials.

Here we focus on toughness mechanisms that can be described by stress-separation relations. The standard small-scale bridging model is as follows (Fig. 5). If condition (5) is

satisfied, the crack can be taken to be semi-infinite compared to the damage zone size L, and the external boundary conditions condensed to stress intensity factor K, or energy release rate $\mathcal{G}$, by handbook solutions. The bridging law (1) is applied in the damage zone, coupled with the elastic solid.

A fiber-reinforced ceramic is characterized in a mechanical test by a resistance curve (R-curve), such as that in Fig. 6. A pre-cut is made prior to a fracture test and, upon loading, a driving force, Γ_0, about the matrix fracture energy, starts matrix crack. As the crack length L increases and more fibers bridge the crack, higher driving force is needed to maintain the growth. The separation at the pre-cut root finally reaches the limiting-separation, $\delta_t = \delta_0$, after which, the damage strip is in a *steady-state*, translating in the body, cracking the matrix in the front, and breaking the fibers in the wake. Quantities of significance on an R-curve are the plateau fracture energy, Γ, and the crack extension to attain the plateau, L_0, which is the length referred to in (5).

Neglecting Γ_0 and assuming a rectilinear bridging law (the rectangle in Fig. 1), Bilby *et al.* (1963) showed that the plateau fracture energy is

$$\Gamma = \sigma_0 \delta_0 , \tag{10}$$

and the steady-state damage zone size is

$$L_0 = \frac{\pi}{8} E' \delta_0 / \sigma_0 . \tag{11}$$

Observe that L_0 scales with the material length $\delta_0 E'/\sigma_0$. As will be shown later, a different bridging law shape χ only modifies the pre-factors in (10) and (11) within order unity. The estimates based on these formulas are listed in Table 1, and discussed below.

Atomic bonds break at a small limiting-separation, amounting to both a small fracture energy and a small damage zone. In practice, condition (5) is always justified, so that LEFM is valid for inherently brittle solids containing cracks longer than a few nanometers.

In contrast, large limiting-separations in fiber bridging lead to both large fracture energies and large damage zones. As indicated in Table 1, the bridging zone size for *fiber pull-out* may violate condition (5), depending on specimen size. The bridging zone size for *fiber cross-over* will certainly violate (5) for most applications.

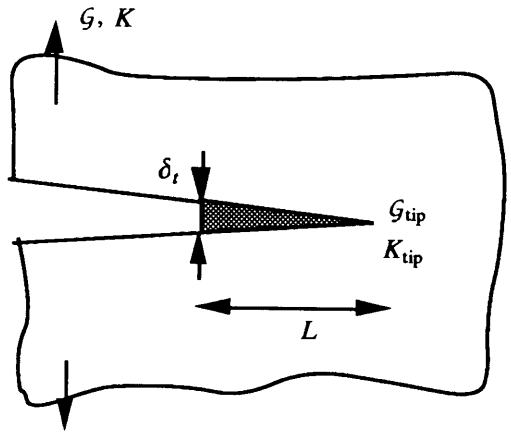

FIG. 5 Small-scale bridging model: the damage is embedded in a K-field, decoupled from the actual component geometry.

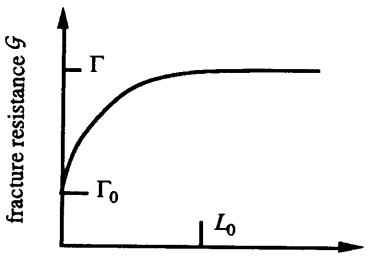

Fig. 6 An R-curve under small-scale bridging conditions.

Given σ_0 and δ_0, (10) and (11) provide estimates for fracture energy and bridging zone size. For example, using (3) and (4) for a fiber-reinforced ceramic, one finds that the fracture energy scales with

$$\Gamma \sim \frac{f(1-f)^2 S_b^3 R}{2E\tau}, \tag{12}$$

and the steady-state bridging zone size scales with

$$L_0 \sim \frac{\pi}{16} \frac{(1-f)^2 S_b R}{f\tau}. \tag{13}$$

Relations of this sort are easy to obtain for other bridging mechanisms, and can serve as a guide for microstructure design. For example, it is clear from (12) that a composite gains high fracture energy from a large fiber strength and radius, but a small sliding friction.

Yet these same quantities also cause a long damage zone. The small-scale damage condition (5) can be combined with (11) to give

$$a/(\delta_0 E'/\sigma_0) \gg 1. \tag{14}$$

The above dimensionless group will appear many times in this article, and provide a focus for discussions. In this context, it measures the *unbridged* crack length, a, in units of material length, $\delta_0 E'/\sigma_0$. Condition (14) is rarely satisfied in practice for a component made of a composite, so toughness is of limited use in design.

1.4 Large-scale bridging

In the recent literature, there is a tendency to report "effective" R-curves, converted from either numerical simulation or experimental record. As demonstrated by Zok and Hom (1990), under large-scale bridging conditions, the R-curves so constructed depend sensitively on specimen geometry and size: they are ineffective and misleading. The practice must be stopped.

Retrospectively, this tendency stems from the success of the concepts related to stress intensity factor in design with metals and ceramics. However, as we will see later in this article, since large-scale bridging is prevalent in composites, many significant concepts in design with, and of, composites, such as strength and notch-brittleness, cannot be deduced from fracture toughness. An all-embracing statement, when large-scale bridging conditions prevail, is that Irwin's one-parameter framework, the classical LEFM, is invalid. To determine load-carrying capacity, a stress analysis is required for *coupled* specimen and bridging law. Consequences of

this statement will be reviewed in Section 3.

2. SMALL-SCALE BRIDGING SOLUTIONS

Small- and large-scale bridging solutions are discussed in detail in this and next section, respectively. The two topics can be read independently, in any order.

2.1 General problem

Now the small-scale bridging model (Fig. 5) is taken up to compute R-curves (Fig. 6). Stress analysis is unnecessary to compute the plateau fracture energy, Γ. An application of Rice's J-integral shows that

$$\mathcal{G} = \mathcal{G}_{tip} + \sigma_0\delta_0\int_0^{\delta_t/\delta_0}\chi(\varepsilon)d\varepsilon, \qquad (15)$$

This equation gives plateau fracture energy Γ when $\delta_t/\delta_0 = 1$ and $\mathcal{G}_{tip} = \Gamma_0$.

A stress analysis is necessary to compute the full R-curve. On dimensional grounds, the separation at the root of the pre-cut takes the form

$$\frac{\delta_t}{\delta_0} = f\left(\frac{L\sigma_0}{\delta_0 E'}, \frac{K}{\sigma_0\sqrt{L}}\right), \qquad (16)$$

and the stress intensity factor at the crack tip

$$\frac{K_{tip}}{\sigma_0\sqrt{L}} = g\left(\frac{L\sigma_0}{\delta_0 E'}, \frac{K}{\sigma_0\sqrt{L}}\right). \qquad (17)$$

Functions f and g will also depend on bridging law shape χ, but nothing else. Integral equations are efficient to solve this class of problems (e.g., Budiansky *et al.* 1988). Observe that K and $\mathcal{G}$, and K_{tip} and $\mathcal{G}_{tip}$ are both related by Irwin's relation (8), so that only two among (15), (16) and (17) are independent.

After f and g are computed, the rising part of the R-curve is given by (17) by letting $K_{tip} = K_0$, and the steady-state bridging zone size L_0 is solved from (16) by letting $\delta_t/\delta_0 = 1$ and $K = K_c = (\Gamma E')^{1/2}$. Explicit solutions are collected in the following sections to assist practitioners in the field.

2.2 Rectilinear bridging law

First consider the rectilinear bridging law (the rectangle in Fig. 1). Specialized from (15), the plateau fracture energy is

$$\Gamma = \Gamma_0 + \sigma_0\delta_0. \qquad (18)$$

The stress analysis gives (Tada *et al.* 1985)

$$K = (8/\pi)^{1/2}\sigma_0\sqrt{L} + K_0. \qquad (19)$$

This equation defines the rising part of the R-curve. The bridging zone size, L_0, is obtained by substituting (18) into (19), giving

$$L_0 = \frac{\pi}{8}E'\frac{\delta_0}{\sigma_0}\left[\left(1+\frac{\Gamma_0}{\sigma_0\delta_0}\right)^{1/2} + \left(\frac{\Gamma_0}{\sigma_0\delta_0}\right)^{1/2}\right]^{-2}. \qquad (20)$$

For the same bridging mechanism, i.e., σ_0 and δ_0 being held constant, the tougher the matrix, the smaller the bridging zone size. When $\Gamma_0/\sigma_0\delta_0 \ll 1$, which is typically the case for fiber-reinforced ceramics, (18) and (20) recover (10) and (11), respectively.

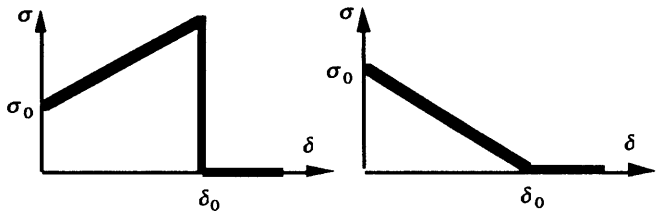

FIG. 7 Bridging laws with hardening and softening.

2.3 Hardening and softening

Consider the stress-separation relation sketched in Fig. 7, having an analytic form

$$\sigma = \begin{cases} \sigma_0 + s\delta, & \delta < \delta_0 \\ 0, & \delta > \delta_0 \end{cases}, \qquad (21)$$

where s is the slope: $s > 0$ for hardening, and $s < 0$ for softening. The shapes are versatile enough to fit many bridging mechanisms, and yet the solutions are simple enough to be tabulated completely. Equation (15) is specialized to

$$\mathcal{G} = \Gamma_0 + \sigma_0\delta_t + \frac{1}{2}s\delta_t^2. \qquad (22)$$

The driving force attains the plateau Γ when $\delta_t/\delta_0 = 1$.

TABLE 2 Hardening Bridging

$8\beta/\pi$	c_2	c_1
0.25	1.244	1.670
0.5	1.478	1.737
1	1.91	1.836
2	2.68	1.984
5	4.44	2.184
10	6.54	2.307
15	8.15	2.356
20	9.51	2.386
25	10.70	2.404
30	11.76	2.414

Once σ_0 is treated as a residual stress, the problem becomes purely linear (e.g., Suo *et al.* 1992a). Linearity and dimensionality dictate that

$$K = c_1\sigma_0\sqrt{L} + c_2K_0, \qquad (23)$$

and that

$$\delta_t = c_3\sigma_0 L/E' + c_4K_0\sqrt{L}/E'. \qquad (24)$$

The pre-factors, c_i, depend only on dimensionless parameter

$$\beta = sL/E'. \qquad (25)$$

Substituting (23) and (24) into (22) gives a quadratic in K_0 and σ_0 being identically zero. This in turn implies that the coefficient of each term in the quadratic vanishes, leading to

$$c_2 = \left(1+2\beta c_1^2\right)^{1/2}, \quad c_3 = (c_2-1)/\beta, \quad c_4 = 2c_1. \qquad (26)$$

That is, all cs are determined if any one of them is.

The hardening spring with $\sigma_0 = 0$ has been solved by Budiansky *et al.* (1988). In present notation, their paper

gives c_2 reproduced in Table 2. Also listed are values of c_1 inferred according to (26).

For many bridging mechanisms, stress rises sharply with a small separation and then decays with a long tail, well fitted by the linear softening triangle in Fig. 7. Bao and Hui (1990) solved the problem when $K_0 = 0$, and their results are listed in Table 3. The solution is now interpreted for the general case with $K_0 \neq 0$, with c_2, c_3 and c_4 obtained from (26).

When $\Gamma_0/\sigma_0\delta_0 \ll 1$, the plateau fracture energy is

$$\Gamma = \frac{1}{2}\sigma_0\delta_0, \tag{27}$$

and the damage zone size upon fracture is

$$L_0 = 0.366E'\delta_0/\sigma_0 \tag{28}$$

These can be compared to (10) and (11) for rectilinear bridging.

TABLE 3 Softening bridging

$-4\beta/\pi$	$2K^2/E'\sigma_0\delta_0$	c_1
0.05	0.192	1.564
0.1	0.366	1.526
0.15	0.521	1.487
0.2	0.657	1.446
0.25	0.771	1.401
0.3	0.864	1.354
0.35	0.933	1.303
0.4	0.978	1.248
0.45	0.998	1.189
0.466	1.000	1.169

To demonstrate the effect of bridging law shape, R-curves calculated using rectilinear and softening laws are contrasted in Fig. 8, both with $\Gamma_0/\sigma_0\delta_0 = 0$. The plateau fracture energy Γ and the strength σ_0 can be measured macroscopically, so they are used to normalize the R-curves. As shown in Fig. 8, given the same Γ and σ_0, the damage zone sizes differ by approximately a factor of 2. R-curves derived from most other bridging laws are expected to be bounded between the two curves in Fig. 8.

2.4 Power-law bridging

Power-law

$$\sigma/\sigma_0 = (\delta/\delta_0)^m \tag{29}$$

embodies fiber pull-out as a special case (m = 1/2), and linear and rectilinear relations as limiting cases (m = 1 and m = 0, respectively). The general solution takes the form

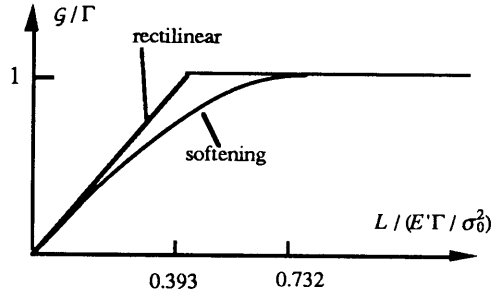

FIG. 8 R-curves due to rectilinear and softening bridging.

$$\delta_t/\delta_0 = \lambda^{1/(1-m)}\Delta\left(\lambda^{-m/(1-m)}K/\sigma_0\sqrt{L}, m\right), \tag{30}$$

and

$$K_{tip}/\sigma_0\sqrt{L} = \lambda^{m/(1-m)}k\left(\lambda^{-m/(1-m)}K/\sigma_0\sqrt{L}, m\right), \tag{31}$$

where

$$\lambda = L/(\delta_0E'/\sigma_0). \tag{32}$$

A scaling relation noted by McMeeking and Evans (1990) and Cox (1992) is used to obtain the above functional forms. Dimensionless functions Δ and k depend on two variables as indicated; they will be tabulated elsewhere (Gu *et al.* 1992).

3. CONSEQUENCES OF LARGE-SCALE BRIDGING

When large-scale bridging prevails, K_c, Γ and R-curve are irrelevant concepts, and load-carrying capacity must be computed by analyzing the component geometry coupled with the bridging law. A large-scale bridging model consists of two elements: derive the bridging law for a candidate material from either micromechanics models or mechanical tests; and compute the load-carrying capacity by analyzing a projected component coupled with the bridging law. Attention here is focused on the latter in a special context: how various mechanical properties, such as strength, notch-ductility and splitting-resistance, can be deduced from bridging laws.

3.1 Dimensionless groups

A dimensionless group appears in *all* large-scale bridging models (see Appendix):

$$\alpha = \frac{a}{\delta_0E'/\sigma_0}. \tag{33}$$

Note that α is the same in (14), but a should be interpreted as a characteristic length of the component. As we shall see, various size effects stem from this dimensionless group.

Design charts can be organized in a nondimensional form. Figure 9 illustrates a panel containing a notch of size a loaded by stress $\bar{\sigma}$. The load-carrying capacity is written

$$\bar{\sigma}_{max}/\sigma_0 = F(\alpha, \Gamma_0/\sigma_0\delta_0). \tag{34}$$

Parameter $\Gamma_0/\sigma_0\delta_0$ measures the relative amount of energy dissipation at the crack tip (e.g., matrix toughness). Also entering (34) are ratios of a to other lengths specifying the component geometry, such as notch root radius and panel width. A different bridging law shape χ only modifies the design curves within order unity, which usually does not affect qualitative conclusions (e.g., notch-brittle or -ductile).

Segregation of the *shape* from the *scale* of a bridging law is of practical significance. Once charts are constructed for idealized bridging laws with important design features (e.g., holes), components with actual bridging laws can be designed, with the charts, by fitting to one of the idealized laws. This approach is equally valuable in design of composites. In this phase, the detailed bridging law shape may be unknown, but the scale of the bridging, σ_0 and δ_0, can be related to microstructural variables. Whether a

material is viable for a particular application can be assessed, before the material is made, by consulting the charts.

The general mechanics problem is stated as follows (Fig. 9). In a body of characteristic length a loaded by stress $\bar{\sigma}$, a matrix crack trajectory of length L is identified, experimentally or hypothetically, emanating from a stress concentrator, bridged according to stress-separation relation (1). The separation at the end of the crack takes the form

$$\delta_t / \delta_0 = f(\bar{\sigma} / \sigma_0, \alpha, L/a), \tag{35}$$

and the energy release rate at the tip

$$\mathcal{G}_{tip} / \sigma_0 \delta_0 = g(\bar{\sigma} / \sigma_0, \alpha, L/a). \tag{36}$$

Functions f and g will also depend on bridging law shape χ, and ratios of a to other lengths characterizing the component geometry. The coupled problem, either linear or nonlinear depending on χ, can be solved by both integral equation and finite element methods. An integral equation using dislocation kernels is derived in Appendix, from which (35) and (36) can be inferred.

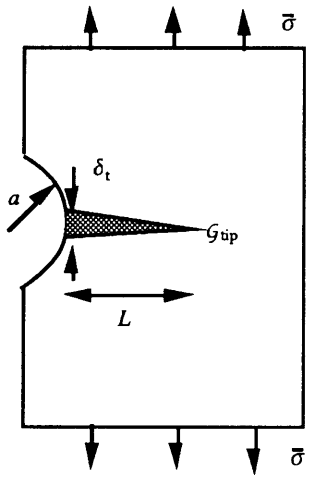

FIG. 9 Large-scale bridging model: the bridging zone is coupled with component geometry.

For rectilinear bridging, linearity dictates that

$$\delta_t E'/a = f_1 \bar{\sigma} - f_2 \sigma_0, \tag{37}$$

and that

$$K_{tip} / \sqrt{a} = f_3 \bar{\sigma} - f_4 \sigma_0, \tag{38}$$

where fs depend on damage extent L/a, and ratios of a over lengths specifying the geometry, but not on α. In particular, when $K_0 = 0$, the above lead to

$$\bar{\sigma}_{max} / \sigma_0 = f_4 / f_3, \tag{39}$$

and

$$\frac{a}{\delta_0 E'/\sigma_0} = \frac{1}{(f_1 f_4 / f_3) - f_2}. \tag{40}$$

This pair gives the function (34), damage extent L/a being regarded as a parameter. Solution for linear softening is still of form (37) and (38), but fs in addition depend on α.

For power-law bridging (29), the solution takes the form

$$\delta_t / \delta_0 = \alpha^{1/(1-m)} \Delta\left(\alpha^{-m/(1-m)} \bar{\sigma} / \sigma_0, L/a\right), \tag{41}$$

and

$$K_{tip} / \sigma_0 \sqrt{a} = \alpha^{m/(1-m)} k\left(\alpha^{-m/(1-m)} \bar{\sigma} / \sigma_0, L/a\right). \tag{42}$$

The dimensionless functions Δ and k also depend on m, and the ratios of a over lengths specifying the geometry, but nothing else (see Appendix). Many solutions of this type have been given by the group at Rockwell International (Marshall *et al.* 1987, Cox and Lo 1992, and Cox 1992).

In obtaining (39) and (40), $\bar{\sigma} / \sigma_0$ is assumed to monotonically increase with L/a, so that the maximum load $\bar{\sigma}_{max} / \sigma_0$ happens at $\delta_t = \delta_0$. This in general is incorrect when $\mathcal{G}_{tip} \neq 0$ (Marshall *et al.* 1987), or the bridging softens (Carpinteri 1990, Bao and Zok 1992). If this seems to be the case, a formal procedure is as follows. After f and g are computed, $\bar{\sigma}_{max}$ is searched as a function of damage extent L/a, subjected to $\mathcal{G}_{tip} = \Gamma_0$ in (35), and $\delta_t \leq \delta_0$ in (36).

Consequences of large-scale bridging are discussed in the following sections. To focus on issues of qualitative significance, the bridging law is assumed to be rectilinear, and the crack tip energy dissipation is negligible, $\Gamma_0 / \sigma_0 \delta_0 = 0$, unless otherwise stated.

3.2 Strength: monolithic solids vs composites

A comparison of the strength of a monolithic ceramic and the strength of a composite is particularly illuminating. Similar comparison has been made by Cottrell (1963) in connection with notch-brittleness.

The strength of a monolithic ceramic measured by a mechanical test, S, is known to be only about a hundredth of the atomic bond strength, σ_0. Griffith (1921) put forth an explanation on a basis of two postulates: 1) atomic debond is the only inelastic process during fracture and, 2) the solid contains traction-free, crack-like flaws comparable to the size of microstructure (e.g., grain diameter). The small-scale damage condition is satisfied: the microstructure is typically on the order of microns, and the atomic debond process is confined within a few nanometers. Crack tips are therefore idealized to be mathematical points in calculating elastic field in the solid. In particular, the energy release rate for a plane strain crack of size $2a$ is (Tada *et al.* 1985)

$$\mathcal{G} = \pi a \bar{\sigma}^2 / E'. \tag{43}$$

Atomic debond absorbs energy $\Gamma = \sigma_0 \delta_0$, as given by (10). The applied stress $\bar{\sigma}$ reaches strength S when $\mathcal{G} = \Gamma$, so that

$$\frac{S}{\sigma_0} = \frac{1}{\sqrt{\pi}} \left(\frac{a}{\delta_0 E'/\sigma_0} \right)^{-1/2}. \tag{44}$$

This curve is indicated by SSB in Fig. 10. Griffith's small-scale bridging model explained the small values of S/σ_0 when $a/(\delta_0 E'/\sigma_0) \gg 1$. However, as clearly indicated in Fig. 10, the model fails when $a/(\delta_0 E'/\sigma_0) \sim 1$, for the strength of a solid should never exceed the atomic bond strength.

For a fiber-reinforced ceramic, the dominant inelastic process is frictional sliding of fiber/matrix interface. Using the illustrative properties in Table 1, assuming that the unbridged flaw size, a, is of a few fiber diameters, one finds that $a/(\delta_0 E'/\sigma_0) < 1$. Consequently, the bridging zone length is comparable to the flaw size, so that the damage zone and the flaw must be analyzed as coupled. The

pertinent results are (Tada *et al.* 1985)

$$\frac{\delta_0 E'}{\sigma_0 a} = 4\left(\eta^2 - 1\right)^{1/2}\left[\frac{\bar{\sigma}}{\sigma_0} - \frac{2}{\pi}\cos^{-1}(1/\eta)\right] + \frac{8}{\pi}\ln\eta, \quad (45)$$

and

$$\frac{K_{tip}}{\sigma_0\sqrt{\pi a}} = \eta^{1/2}\left[\frac{\bar{\sigma}}{\sigma_0} - \frac{2}{\pi}\cos^{-1}(1/\eta)\right], \quad (46)$$

where $\eta = 1 + L/a$.

The strength $\bar{\sigma} = S$ is obtained by setting $\delta_t = \delta_0$ and $K_{tip} = 0$:

$$\frac{8}{\pi}\left(\frac{a}{\delta_0 E'/\sigma_0}\right)\ln\left[\sec\left(\frac{\pi}{2}\frac{S}{\sigma_0}\right)\right] = 1. \quad (47)$$

This equation is indicated by LSB in Fig. 10. A comparison of the two curves gives a quantitative feel for the regime where the small-scale bridging assumption is valid. Indeed, the LSB model predicts that S/σ_0 approaches unity when the unbridged flaw size a is small, as anticipated. Since typically $a/(\delta_0 E'/\sigma_0) \sim 1$ for a composite, the strength of a composite is insensitive to processing defects, as compared to the strength of a monolithic ceramic.

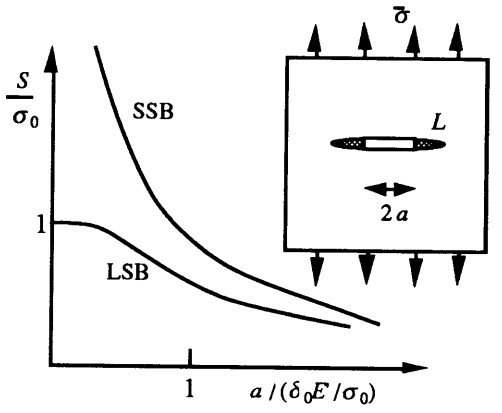

Fig. 10 Strength predicted by small- and large-scale bridging. The former is correct only when a is large.

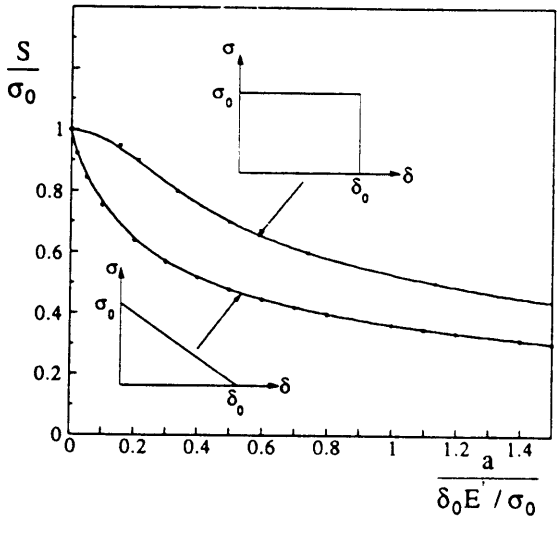

Fig. 11 Strength of a material computed from rectilinear and softening bridging laws.

To demonstrate the effect of bridging law shape, Fig. 11 plots strength computed from rectilinear and softening bridging laws (Bao and Zok 1992). The difference is appreciable, but of order unity. When a proper selection of σ_0 and δ_0 is made, bridging laws of other shapes would give rise to strength bounded between the two curves in Fig. 11.

3.3 Notch-sensitivity

Holes are often drilled in a panel for fastening or cooling. Neither toughness nor strength can be directly used to determine the maximum static load. However, a designer knows to ignore a small hole in a ductile metal panel, but not a hole in a ceramic. What about a fiber-reinforced ceramic? To fix the idea, Fig. 12 illustrates a panel with a hole, and the question is how much load the panel can carry.

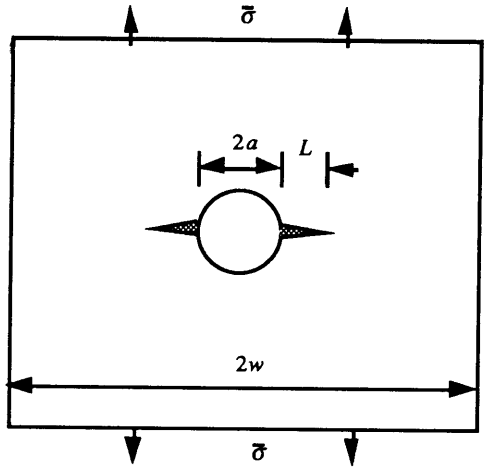

FIG. 12 A panel containing a hole.

The answer depends on materials. For a monolithic ceramic panel, the load should be such that the stress at the hole is below the "strength" of the ceramic. Let σ_0 be a reference value of strength (ignoring statistical distribution), and C be the stress concentration factor at the hole. The maximum load that can be carried by the panel is given by

$$\bar{\sigma}_{max}/\sigma_0 = 1/C. \quad (48)$$

The stress concentration factor depends on a/w (Peterson 1971); Equation (48) is plotted in Fig. 13. Notice that even a small hole ($a/w = 0$) reduces the load-carrying capacity by a factor of 3: ceramics are *notch-sensitive*.

The design criterion is different for a ductile metal panel under static load. Plasticity relieves stress concentration near the hole, so that the maximum load should be such that the net section fully yields:

$$\bar{\sigma}_{max}/\sigma_0 = 1 - a/w, \quad (49)$$

where σ_0 is the yield strength of the metal. Equation (49) is plotted in Fig. 13. A small hole does not reduce much load-carrying capacity: ductile metals are *notch-insensitive*.

What about a panel made of a fiber-reinforced ceramic? The answer depends on material *and* hole size. Matrix cracking near the hole, allowing fibers to slide, provides a mechanism for ductility δ_0 and stress redistribution. The

composite behaves according to the dimensionless group

$$\frac{a}{\delta_0 E'/\sigma_0} = \begin{cases} 0, & \text{notch-ductile} \\ \infty, & \text{notch-brittle} \end{cases} \quad (50)$$

That is, notch-sensitivity is a property of both material *and* notch size: for a given composite, a large hole tends to be ceramic-like, but a small hole metal-like. In practice, δ_0 can be changed, by orders of magnitude, by varying the sliding friction. Such experiments would verify the model.

Classification (50) emerges directly from the dimensional analysis of the large-scale bridging model (see Appendix). Another dimensionless group, $a/\left(\Gamma E'/\sigma_0^2\right)$, has long been used to correlate transition behaviors for metals (see Kanninen and Popelar 1985). The two groups are equivalent since $\Gamma \sim \delta_0\sigma_0$. Large-scale bridging concepts provide a framework to simulate notch brittle-to-ductile transition behaviors for composites. As we shall see, some behaviors have close analogues in metals, others do not.

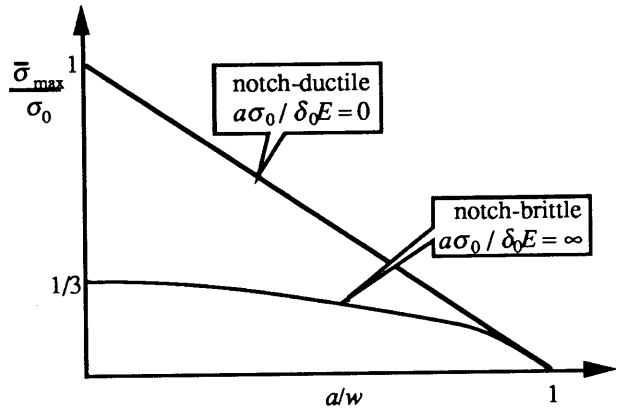

FIG. 13 The maximum load for a panel containing a hole.

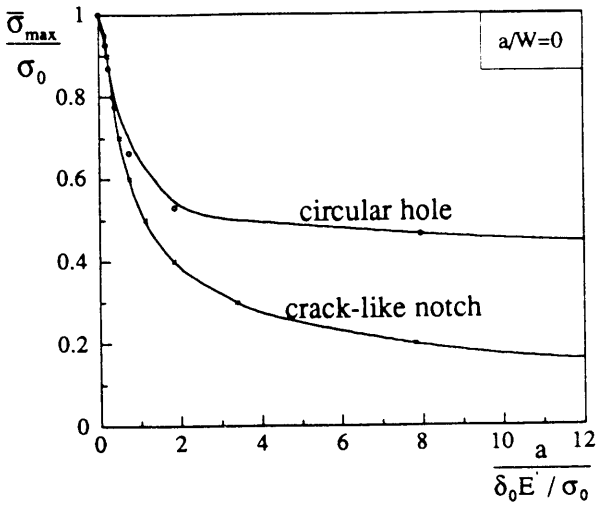

Fig. 14 Notch ductile-to-brittle transition (Ho and Suo 1992).

The maximum loads for intermediate values of $(a\sigma_0)/(\delta_0 E)$ fall in between the two limiting curves in Fig. 13, which can be computed by invoking large-scale bridging concepts. Figure 14 plots the results of such a computation for a hole in a large panel ($a/w = 0$). Specifically, the hole becomes notch-brittle when $a/(\delta_0 E'/\sigma_0) > 10$. For example, for a composite with $\delta_0 E'/\sigma_0 \sim 1$ mm, a hole of a centimeter radius will be notch-brittle. The mechanics model to construct Fig. 14 is similar to that in Section 3.2, except that finite elements are used to compute fs in (37) and (38).

Also included in Fig. 14 is the maximum load for a panel containing a crack-like notch (Eq. 47). The two are expected to bound the curves for notches of various root radii. Computations on the effects of notch radius and elastic orthotropy are in progress (Gu *et al.* 1992).

Notch-ductility can be enhanced by various damage modes, notably, multiple cracking and matrix splitting along the fiber direction. To illustrate, consider a hole with splits (Fig. 15). The extent of the splits, h/a, is determined by the shear resistance $\hat{\tau}$, resulting from either friction in unidirectional composites, or bending of 90 degree fibers in woven composites. The anticipated results are sketched in Fig. 16. When $\hat{\tau}/\sigma_0 \sim 0$, the splits are long and the matrix crack becomes an edge crack, so that the full load-carrying capacity can be reached. When $\hat{\tau}/\sigma_0 \sim \infty$, the splits are small, so that the curve in Fig. 14 is reached. Detailed results will be reported elsewhere (He and Suo 1992).

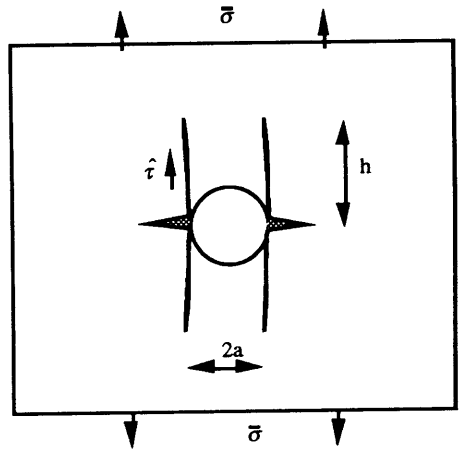

FIG. 15 A stress concentrator (the hole) relaxed by splits.

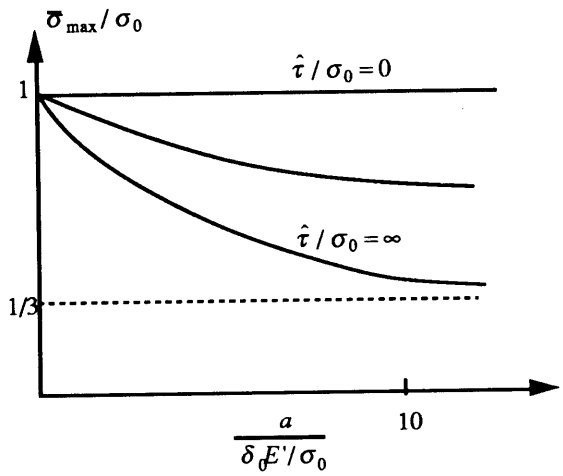

FIG. 16 Notch-ductility due to splitting.

3.4 Transverse cracks: Splitting vs tunneling

Two types of transverse cracks, splitting and tunneling, are illustrated in Figs. 17 and 18. They take the same fracture path in the matrix, along the fiber direction, with fibers crossing over the crack plane. For splitting, the cross-over fibers supply substantial fracture resistance *in addition to* matrix fracture energy (Spearing and Evans 1992). In contrast, the cross-over fibers provide little resistance to tunneling cracks (Beyerle *et al.* 1992). As we shall show, this is a large-scale bridging effect.

To understand the difference, first consider a splitting beam of thickness $2h$, bridged over length L, and loaded by moment M (Fig. 17). Typically L is comparable to $2h$, but smaller than the total crack length. The problem has been analyzed by Suo *et al* (1992a); the results pertinent to the present discussion are outlined below.

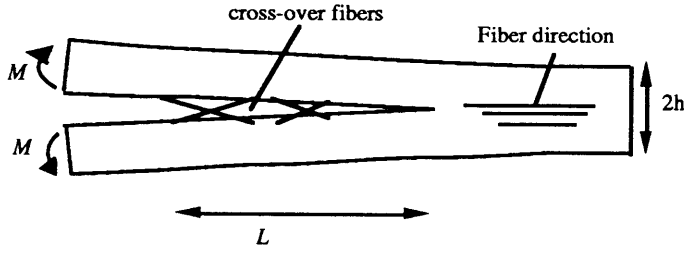

FIG. 17 A splitting beam interacting with cross-over fibers.

An application of the J-integral shows that

$$12M^2/E'h^3 = \sigma_0\delta_t + \Gamma_0, \qquad (51)$$

where the left-hand side is the integral computed over the external boundary of the beam, and the right-hand side over the bridging zone. The crack tip energy dissipation, Γ_0, is also included for the sake of discussion. The maximum moment is reached when $\delta_t = \delta_0$:

$$12M_{\max}^2/E'h^3 = \sigma_0\delta_0 + \Gamma_0. \qquad (52)$$

Using the illustrative numbers in Table 1 and the typical value for a glass matrix, $\Gamma_0 \sim 10$ J/m^2, one finds that the cross-over fibers substantially increases $M_{\max}$. Since it is small, Γ_0 is to be ignored in the following estimate of the bridging zone size.

The disturbing number in Table 1, $L_0 = 1$ m, is predicted from the small-scale bridging model. It is incorrect: L of a few beam thickness, about several centimeters, is observed in experiments. The flexibility of a beam can substantially reduce the critical bridging zone length. This is a large-scale bridging effect, as shown below.

Dimensional considerations lead to

$$M = \frac{1}{2}a_1L^2\sigma_0, \qquad (53)$$

where a_1 depends only on L/h, and is of order unity when $L/h > 1$ (Suo *et al.* 1992a). Combination of (52) and (53) gives the critical bridging zone length when $\delta_t = \delta_0$:

$$L_0 = a_1^{-1/2}(E'\delta_0/3\sigma_0)^{1/4}h^{3/4}. \qquad (54)$$

For example, with $h = 1$ cm, one finds $L_0 = 3$ cm, suggesting that the potential fracture resistance can be realized in beams with practical size.

The J-integral over the external boundary of the beam can be interpreted as the driving force for splitting. Figure 19 plots J as a function of matrix crack extension, L, where (53) is the rising part, and (52) the plateau. In contrast to the R-curves under small-scale bridging conditions, the J-L curves depend on beam thickness. The latter are therefore *not* material properties.

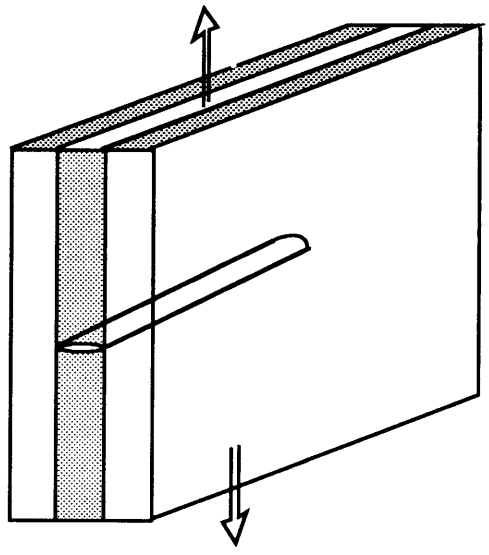

FIG. 18 A crack tunneling in a 90°-ply.

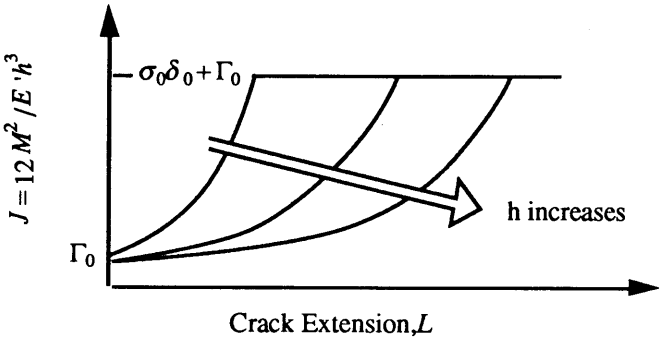

FIG. 19 J-integral as a function of crack extension, L, and beam thickness, h.

Cross-over fibers do not provide much resistance to tunneling cracks (Beyerle *et al.* 1992). A large crack separation is a prerequisite for using the large limiting-separation δ_0 (~ 100 μm), which cannot be realized in a tunnel constrained by the surrounding material. Consequently, tunneling cracks are only resisted by matrix fracture energy Γ_0. A mechanics model for tunneling cracks is given by Ho and Suo (1991)

3.5 A note on measuring bridging law

Various methods have been considered to determine the bridging law from either experiments, models, or combinations (Cox 1991). One such method is described as follows (Li *et al.* 1987).

Write a bridging law as

$$\sigma = \sigma(\delta). \tag{55}$$

Rice (1968) showed that

$$J = J_{tip} + \int_0^{\delta_t} \sigma(\delta) d\delta, \tag{56}$$

where J is the J-integral computed over a contour outside the bridging zone, J_{tip} over a contour close to the crack tip, and δ_t the separation at the pre-cut root (Fig. 20). Upon loading, $J_{tip} = \Gamma_0$ is maintained as the matrix crack extends. Differentiating (56) with respect to δ_t gives

$$\sigma(\delta_t) = \partial J / \partial \delta_t. \tag{57}$$

Consequently, the bridging law can be determined if both J and δ_t can be determined as a function of applied load P. Since the limiting-separation for various bridging mechanisms in composites is in the range 10 ~ 100 μm, many experimental techniques may be used to measure δ_t *in situ*.

Difficulty arises to relate J to the applied load P. There has been a misconception that J is related to P through handbook solutions for K. This is wrong since Irwin's relation (8) is valid only under small-scale bridging conditions. Under large-scale bridging conditions, J usually depends on the bridging law, which is yet to be determined from the very experiment. A procedure has been proposed by Li *et al.* (1987) to determine J experimentally. In general, the method suggested by (57) will be difficult to use under large-scale bridging conditions.

There are exceptions. For example, the J-integral over the external boundary of a splitting beam (Fig. 17) is independent of the bridging law (Rice 1968):

$$J = 12M^2 / E' h^3. \tag{58}$$

Thus, splitting beam can be used to determine the bridging law under large-scale bridging conditions. Specimens having the same attribute are reviewed by Suo *et al.* (1992a).

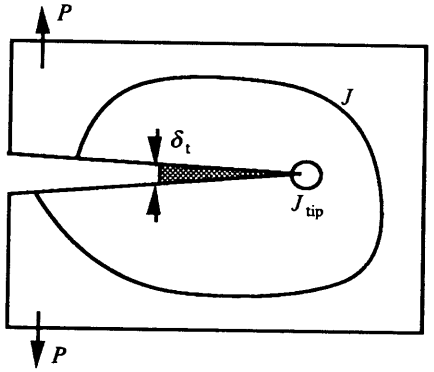

FIG. 20 Contours over which J-integrals are computed.

4. SUMMARY

Figure 21 summarizes the main theme of crack-bridging concepts. At the center is the bridging law, derived from micromechanics models and experiments, which, combined with continuum stress analysis, gives rise to mechanical properties such as toughness, strength, notch-ductility. Consequently, bridging law (1) replaces toughness or strength as the basic material property. Together with an elastic component, the bridging law provides a length, $\delta_0 E'/\sigma_0$, varying from a nanometer to a meter for different bridging mechanisms (Table 1), which is responsible for the vast differences in failure behaviors. Large-scale bridging introduces a dimensionless group, $a/(\delta_0 E'/\sigma_0)$, where a is the length characterizing a component, having different meanings in various contexts: unbridged crack size for toughness, unbridged flaw size for strength, and hole radius for notch-sensitivity. It is demonstrated that the set of normalization introduced in this article separates the roles played by the shape and the scale of a bridging law, so that a design chart can be presented in a nondimensional form (34), and a different bridging law only modifies the chart within order unity. A collection of small-scale bridging solutions is given in Section 2 for several idealized bridging laws. Large-scale bridging effects are illustrated in Section 3 by examples of practical significance.

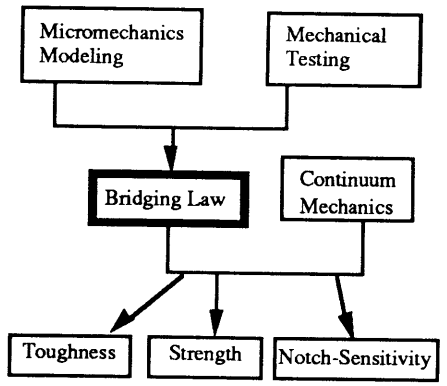

FIG. 21 The main theme of crack-bridging concepts.

ACKNOWLEDGEMENTS

ZS is grateful for the financial support of NSF grant MSS-9011571, and of DARPA University Research Initiative, ONR Contract N00014-86-k-0753.

REFERENCES

Bannister M, Shercliff H, Bao G, Zok FW and Ashby MF (1992) Toughening in brittle systems by ductile bridging ligaments, *Acta Metall. Mater.*, in press.

Bao G and Hui CY (1990) Effects of interface debonding on the toughness of ductile-particle reinforced ceramics. *Int. J. Solids Structure*, 26, 631-642.

Bao G and Zok FW (1992) On the strength of particle reinforced brittle matrix composites. Manuscript in preparation.

Beyerle DS, Spearing SM and Evans AG (1992) Damage mechanisms and the mechanical properties of laminated 0/90 ceramic-matrix composites. Submitted to *J. Am. Ceram. Soc.*

Bilby BA, Cottrell AH and Swinden KH (1963) The Spread of Plastic Yield from a Notch, *Proc. Roy. Soc. Lond.* A272, 304-314.

Budiansky B, Amazigo JC and Evans AG (1988) Small-scale crack bridging and the fracture toughness of particulate reinforced ceramics. *J.*

Mech. Phys. Solids. 36, 167-187.

Carpinteri A (1990) A catastrophe theory approach to fracture mechanics, *Int. J. Fracture*, 44, 57-69.

Cottrell AH (1963) Mechanics of fracture, *Tewksbury Symposium on Fracture*, 1-27, University of Melbourne. (1975) Fracture, in *The Physics of Metals, 2. Defects*, Ed P.B. Hirsch, Cambridge University Press, New York.

Cox BN (1991) The determination of crack bridging forces, *Int. J. Fracture*. In press.

Cox BN (1992) Scaling for bridged cracks. Submitted to *J. Appl. Mech.*

Cox BN and Lo CS (1992) Load ratio and notch effects for bridged fatigue cracks in fibrous composites. *Acta Met. Mater*. 40, 69-80.

Dugdale DS (1960) Yielding of steel sheets containing slits, *J. Appl. Mech.*, 8, 100-104.

Dundurs J (1968) Elastic interaction of dislocations with inhomogeneities, in *Mathematical Theory of Dislocations*, 70-115, ASME, New York.

Evans AG (1990) Perspective on the development of high-toughness ceramics, *J. Am. Ceram. Soc.* 73, 187-206.

Griffith AA (1921) The phenomena of rupture and flow in solids, *Phil Trans. Roy. Soc. Lond.* A221, 163-197.

Gu P, Shih CF and Suo Z (1992) Toughness and notch sensitivity of composites having power-law bridging. Work in progress.

He MY and Suo Z (1992) Notch sensitivity and splitting. Work in progress.

Ho S and Suo Z (1991) Tunneling cracks in constrained layers. Submitted for publication.

Ho S and Suo Z (1992) Notch brittle-to-ductile transition in metal and ceramic matrix composites. Work in progress.

Hutchinson JW and Jensen HM (1990) Models of fiber debonding and pullout in brittle composites with friction. *Mech. Mater.* 9, 139-163.

Irwin GR (1957) Analysis of stresses and strains near the end of a crack traversing a plate, *J. Appl. Mech.* 24, 361-364.

Kanninen MF and Popelar CH (1985) *Advanced Fracture Mechanics*. Oxford University Press, New York.

Li VC (1990) Non-linear fracture mechanics of inhomogeneous quasi-brittle materials, in *Nonlinear Fracture Mechanics*, ed. MP Wnuk, Springer-Verlag, New York.

Li VC, Chan CM and Leung KY (1987) Experimental determination of the tension-softening relations for cementitious composites, *Cement and Concrete Research*, 17, 441-452.

Marshall DB, Cox BN and Evans AG (1985) The mechanics of matrix cracking in brittle matrix composites, *Acta Metall.* 33, 2013-2021.

Marshall DB and Cox BN (1987) Tensile fracture of brittle matrix composites: influence of fiber strength, *Acta Metall.* 35, 2607-2619.

Mataga PA (1989) Deformation of crack-bridging ductile reinforcements in toughened brittle materials, *Acta Metall.*, 37, 3349-3359.

McMeeking RM and Evans AG (1990) Matrix fatigue cracking in fiber composites. *Mech. Mater.* 9, 217-227.

Needleman A (1990). An analysis of tensile decohesion along an interface, *J. Mech. Phys. Solids*, 38, 389-324.

Peterson RE (1974). *Stress Concentration Factors*. John Wiley, New York.

Rice JR (1968) A path independent integral and the approximate analysis of strain concentrations by notches and cracks, *J. Appl. Mech.* 35, 379-386.

Ritchie RO and Thompson AW (1985) On macroscopic and microscopic analysis for crack initiation and crack growth toughness in ductile alloys. *Met. Trans.* 16A, 233-247.

Spearing SM and Evans AG (1992) The role of fiber bridging in the delamination resistance of fiber-reinforced composites, *Acta Metall. Mater*. In press.

Suo Z, Bao G and Fan B (1992a) Delamination R-curves due to damage. *J. Mech. Phys. Solids*. 40, 1-16.

Suo Z, Ortiz M and Needleman A (1992b) Stability of solids with interfaces, *J. Mech. Phys. Solids*. In press.

Tada H, Paris PC and Irwin GR (1985) *The Stress Analysis of Cracks Handbook*. Del Research, St. Louis, MO.

Zok FW and Hom CL (1990) Large scale bridging in brittle matrix composites, *Acta Metall. Mater*. 38, 1895-1904.

APPENDIX

A crack, traction-free or bridged, is equivalent to an array of continuously distributed dislocations (Bilby *et al.* 1963). The dislocation per unit length, b, is related to crack separation, δ, by

$$b(x) = -\partial\delta / \partial x. \qquad \text{(A1)}$$

Resulting from geometric considerations, this has nothing to do with pile-up dislocations in a real crystal. Solutions to a single dislocation interacting with a hole, a free surface, or a crack are available in the literature, which can be used as kernels to formulate integral equations for notch-sensitivity problems (Gu *et al.* 1992).

To illustrate, consider a hole in an infinite composite (Fig. 12, a/w = 0). The stress prior to matrix cracking is given by the standard elasticity solution of a hole in an infinite plate:

$$\sigma(x) = \bar{\sigma} F(x / a), \qquad \text{(A2)}$$

where $\bar{\sigma}$ is the applied stress, and dimensionless function F is given in elasticity textbooks. The stress induced by a pair of edge dislocations, symmetrically located at $x = \pm \xi$, is given by

$$\sigma(x) = \frac{E'}{a} H(x / a, \xi / a) b(\xi), \qquad \text{(A3)}$$

where H is a known function (Dundurs 1968).

Superimposing the stress due to the dislocations and the remote stress leads to

$$\sigma_0 \chi(\delta / \delta_0) = \bar{\sigma} F - \frac{E'}{a} \int_a^{a+L} H \frac{\partial \delta}{\partial \xi} \mathrm{d}\xi \qquad \text{(A4)}$$

The bridging law (1) is also incorporated in the above. Equation (A4) is the integral equation governing crack separation $\delta(x)$, to be solved numerically. Normalizing (A4) according to

$$\bar{\sigma} / \sigma_0,\ \delta / \delta_0,\ x / a,\ L / a, \qquad \text{(A5)}$$

one can confirm (35) and (36) for any bridging law, and (41) and (42) for power-law.